Bioprinting 20 (2020) e00092

Contents lists available at ScienceDirect

Bioprinting

journal homepage: www.elsevier.com/locate/bprint

Assessment of coaxial printability for extrusion-based bioprinting of alginate-based tubular constructs

Myoung Hwan Kim [a,b], Seung Yun Nam, Ph.D. [c,d,*]

[a] Department of Biomedical Engineering, Pennsylvania State University, University Park, PA, USA
[b] The Huck Institutes of the Life Sciences, Pennsylvania State University, University Park, PA, USA
[c] Department of Biomedical Engineering, Pukyong National University, Busan, South Korea
[d] Center for Marine-Integrated Biomedical Technology (BK21 Plus) Pukyong National University, Busan, South Korea

ARTICLE INFO

Keywords:
Bioprinting
Coaxial printing
Printability
Shape fidelity
Biomaterials

ABSTRACT

Coaxial printing has emerged as a versatile technique of bioprinting for better capability in tissue engineering by allowing the injection of two materials having different mechanical and biochemical properties in two distinct layers. Thus, coaxial printing can enhance mechanical properties as well as biological activities in a coaxial structure. However, despite these advantages of coaxial printing, there was no experimental study regarding the evaluation of coaxial printability and shape fidelity for extrusion-based bioprinting. In this study, we quantitatively investigated coaxial printability and shape fidelity of the coaxial-printed scaffolds using alginate and Pluronic F-127 which are the most widely used biomaterials for bioprinting. With the optimal concentrations of calcium chloride for alginate, a 3D tubular structure with high shape fidelity could be directly fabricated using core-crosslinking method. The presented results suggest a methodological solution to improve the coaxial printability for various tissue engineering applications using coaxial bioprinting.

1. Introduction

Recently, numerous techniques for maximizing the efficacy of bioprinting have been developed in the field of tissue engineering and regenerative medicine [1–3]. Among these techniques, coaxial printing is a versatile method which can combine various biomaterials, cells, and crosslinking agents in two distinct layers often called shell and core [4–6]. Various combinations of biomaterials for better capability in tissue regeneration can be simultaneously extruded in the coaxial filament. Hence, the coaxial-printing of two materials with different mechanical and biochemical properties can create a synergistic effect on printability, structural complexity, shape fidelity, and biocompatibility. In general, scaffolds with stiff biomaterials have optimal shape fidelity for printing, but the high stiffness of the material can have a negative effect on biological activities of the encapsulated cells in the scaffolds [7]. In contrast, scaffolds with relatively poor mechanical properties can provide microenvironments suitable for cell viability and proliferation [8], but it has a restriction in fabricating well-constructed 3D structures [7,9]. Therefore, it is challenging to design and develop bioinks which can meet various needs in tissue engineering and regenerative medicine. Coaxial printing is a way to overcome the current limitations of bioprinting by allowing users to select multiple biomaterials according to specific purposes. For instance, in coaxial printing, a stiffer material could be included in the core for mechanical support while a relatively weak material can be located in the shell for biological activities [10,11]. Thus, coaxial printing has a great potential for a useful tool to provide robust overall mechanical properties as well as biological activities in a simply designed structure.

In addition, coaxial printing has been widely used to fabricate hollow or tubular structures. Due to the ability to deliver nutrients, oxygen, and other biochemical components through the core part, coaxial-printed tubular constructs can mimic natural vascular networks [12–14]. Also, the superiority of the coaxial-printed scaffolds over single-nozzle printed scaffolds was recently demonstrated in terms of the biological activities such as cell-scaffold interaction, migration, proliferation, and even angiogenesis from soft to hard tissues [5,10,15,16]. However, despite these advantages of coaxial printing, there was no experimental study regarding the evaluation of coaxial printability and shape fidelity indicating the stability of the coaxial-printed structure based on material extrusion. To fabricate 3D-printed structures with high fidelity and precise positioning, printability is one of the most important factors in extrusion-based bioprinting [17,18]. Especially in coaxial printing, the

* Corresponding author. Department of Biomedical Engineering, Pukyong National University, 45, Yongso-ro, Nam-gu, Busan, 48513, South Korea.
E-mail address: synam@pknu.ac.kr (S.Y. Nam).

https://doi.org/10.1016/j.bprint.2020.e00092
Received 17 April 2020; Received in revised form 21 July 2020; Accepted 22 July 2020

optimization of the printability is essential due to the complex geometry of coaxial-printed structures using two different properties of biomaterials loaded in the shell and core parts [19].

In this study, coaxial printability and shape fidelity of the coaxial-printed scaffolds were quantitatively assessed using tubular scaffolds fabricated using pluronic F-127 in the core and alginate in the shell. Pluronic F-127 has an excellent printability and is used as a sacrificial material for various applications, especially in the tubular constructs due to its thermo-reversibility [20,21]. In addition, alginate is one of the widely used materials in pharmaceutical and biomedical applications as well as in microfluidic spinning because of its biocompatibility and simple ionic crosslinking with calcium ions [22–25]. Hence, we demonstrate a newly developed core-crosslinking method to fabricate a coaxial-printed scaffold that consists of the two previously mentioned materials. The optimal concentrations of calcium chloride added in the shell and the core as a crosslinking agent for alginate are comprehensively suggested. Moreover, the coaxial printability and shape fidelity of the coaxial-printed scaffold with different concentrations of calcium chloride were monitored using rheological characterization, microscopic images, and the filament collapse test. Lastly, we compared the structural superiority of coaxial-printed structure to the conventional crosslinking method. Therefore, this study can offer a methodological approach not only to improve but also to optimize the coaxial printability and shape fidelity for various applications in tissue engineering and regenerative medicine.

2. Materials and methods

2.1. Preparation of hydrogel

Sodium alginate (Alg) extracted from brown algae was purchased from Sigma-Aldrich Inc. and the Alg solution was fixed at 2.5% (w/v) as the final concentration. The Alg solution was pre-crosslinked with several concentrations (0.1, 0.2, 0.3, 0.4, and 0.5% w/v) of calcium chloride ($CaCl_2$, Reagents Duksan Inc., Korea) to determine the optimal concentration for extrudability as the shell material. Pluronic F-127 (F127, Sigma-Aldrich Inc., USA) of 30 wt% was prepared and used for the core material. The F127 contained high concentrations of $CaCl_2$ (1, 3, 5 and 10% w/v) to crosslink the Alg solution immediately after extrusion. Red dye (0.1 wt% new coccine, Sigma-Aldrich Inc. USA) was added to F127 for visualization of the coaxial-printed structure. All solutions were dissolved in deionized water purified by RiOs™ (Millipore, France). The shell and core materials enabled curing for at least 30 min before experiments.

2.2. Rheological evaluation

The rheological properties of the shell and core materials were measured using a rheometer (HR-2, TA Instruments Inc., USA). All the rheological experiments were performed in triplicates with a 20 mm parallel plate at 25 °C. Frequency sweep test was carried out to evaluate the storage modulus (G') and the loss modulus (G") of samples in ranging from 0.1 to 100 rad/s at a strain in the linear viscoelastic region. The shear moduli of the samples were compared at the angular frequency of 1 rad/s in the graph of the angular frequency-shear modulus. Temperature sweep test for sol-gel transition temperature of F127 was achieved at a range of 0–50 °C with 1 °C temperature step.

2.3. Coaxial printing

The coaxial needle having different diameters of 330 μm and 1070 μm for the inner and outer needles respectively as shown in Fig. 1(a) was attached to the custom-made 3D bioprinting system composed of the multi-printing head with independent pneumatic controllers (<700 kPa) and temperature controllers (<200 °C). The F127 containing $CaCl_2$ was included in the core while alginate pre-crosslinked with $CaCl_2$ was located in the shell for the coaxial printing as shown in Fig. 1(b). The coaxial printing was conducted with a pressure of extrusion ranging from 150 to 160 kPa to the core material and from 50 to 140 kPa to the shell material. The printing velocity was fixed at 5 mm/s.

2.4. Filament collapse test

The filament collapse test represents the extent of sagging of the printed filament on a model with 1, 2, 4, 8, and 16 mm spacing fabricated by a FDM-based 3D printer (3DWOX 1, Sindoh, Korea) with ABS material [26–28]. A coaxial-printed filament was printed on the model and observed with the time elapsed (0, 30, 60 and 120 s) after printing. The degree of sagging was analyzed using NIH Image J software (National Institute of Health, USA). The values were color-mapped to clearly represent the degree of sagging.

2.5. Morphological characteristics

To evaluate coaxial printability, a straight line of the coaxial-printed filament was observed using a microscope. The shape fidelity was assessed with a 21.12 mm × 21.12 mm square-shaped coaxial printed structure with two layers and six layers. The printed structure was soaked in phosphate buffered saline (PBS, Corning Inc. USA) and F127 was

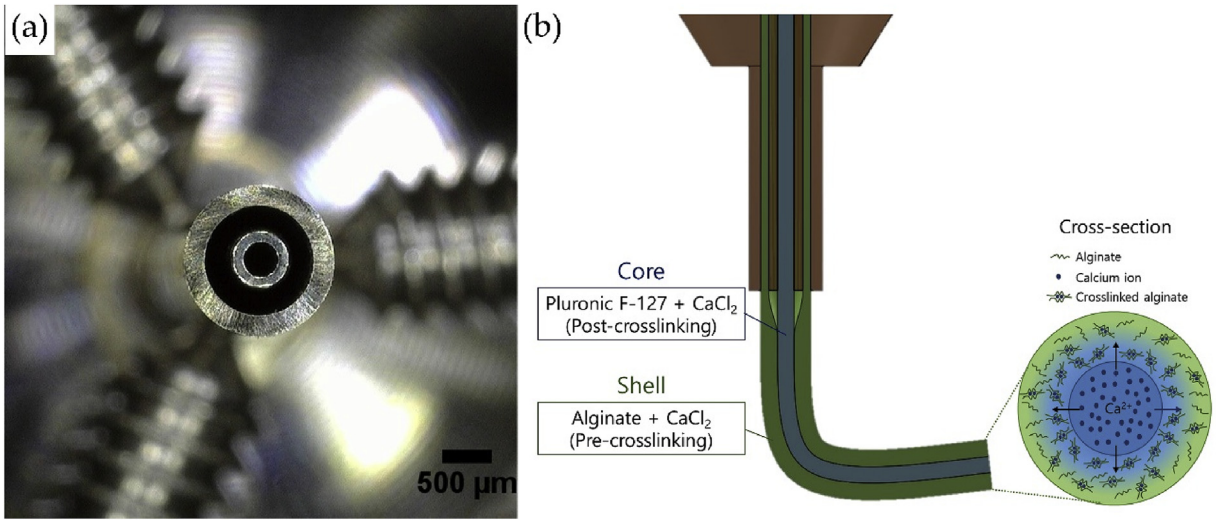

Fig. 1. (a) Coaxial nozzle; (b) Schematic of the coaxial printing.

removed from the core material in the structure by cooling in a refrigerator around at 4 °C for an hour. After removal of the core material, macro and microscopic images were taken.

To demonstrate the suitability of the presented method (core-crosslinking method) for the coaxial printing, conventional method [29–31] and core-crosslinking method were compared as the post-crosslinking to Alg for the coaxial printing. For the conventional method, as the post-crosslinking, 5% $CaCl_2$ (non-included in F127) was treated to the coaxial-printed scaffold for a minute after printing. The core-crosslinking method used F127 contained with 5% $CaCl_2$ in the core material. Both experiments were monitored after for removal of the core material as mentioned above.

3. Results

3.1. Rheological properties and extrudability

To validate the influence of $CaCl_2$ on the rheological properties of the hydrogel, varying concentrations of $CaCl_2$ were added to Alg and F127 for the shell and core materials respectively. In general, the low concentration of $CaCl_2$ for pre-crosslinking enables Alg to extrude by increasing shear modulus and viscosity [32,33]. Likewise, as shown in Fig. 2(a), shear moduli of the Alg hydrogel crosslinked with $CaCl_2$ for the pre-crosslinking were augmented with increasing $CaCl_2$ concentrations. However, due to excessive crosslinking, extrudable Alg hydrogel was difficult to prepare with more than 0.4% of $CaCl_2$. Fig. 2(b) (detail with video in Video S1, Supplementary Materials) shows extrudability of crosslinked Alg-$CaCl_2$ hydrogel at a pressure of 200 kPa using a single nozzle with an inner diameter of 340 μm. The extrudability of the Alg--$CaCl_2$ hydrogel was adequate until crosslinking with 0.3% $CaCl_2$ and then it was inappropriate as a result of clogging caused by over-crosslinked Alg solution. Therefore, concentrations over 0.4% $CaCl_2$ were not selected for further experiments. In fact, various studies [18,34] using pre-crosslinked Alg hydrogel were performed with 0.2% $CaCl_2$.

Supplementary video related to this article can be found at https://doi.org/10.1016/j.bprint.2020.e00092

Next, the rheological properties of F127 with high concentrations of $CaCl_2$, as the core material, were measured. F127 exists in the liquid state at low temperature, while gelating at body temperature [35]. The presence of $CaCl_2$ on F127 has slight effects on rheological properties such as shear modulus and sol-gel transition temperature result from the solubility of F127. Fig. 2(c) shows shear moduli (G') between two different temperatures i.e. 25 °C and 37 °C according to the $CaCl_2$ concentrations. Loss moduli (G") indicating viscous property as represented shows a slight increase with the different temperatures and the concentrations of $CaCl_2$. Storage moduli at 0% $CaCl_2$ show increase at 37 °C due to the thermos-reversibility property of F127. Further, with an increase in the concentration of $CaCl_2$ (1, 3, 5, and 10%), the difference between the shear moduli at 25 °C and 37 °C becomes reduced. The phenomenon has been reported that the inorganic salt such as $CaCl_2$ has an inclination to have more familiar with water molecules than polymer molecules such as F127 composed of triblock copolymer poly(ethylene oxide)-poly(propylene oxide)-poly(ethylene oxide) [36]. Thus, these properties can lead to the reduction of shear modulus and sol-gel transition temperature due to deficient of bonding between water and polymer molecules. The sol-gel transition temperature as shown in Fig. 2(d) was decreased with increasing the concentration of $CaCl_2$. The results of rheological properties of $CaCl_2$ included F127 were considered for selecting optimal printing parameters for further experiments.

3.2. Coaxial printability of the filament

Printability of the coaxial-printed filament with the distinctively colored shell and core materials was assessed using microscopic images. In Fig. 3, the shell material without $CaCl_2$ (Alg 2.5% + $CaCl_2$ 0.0%) did not clearly appear due to low shear moduli regardless of the concentration of $CaCl_2$ in the core material. In the figures with the shell material with Alg 2.5% + $CaCl_2$ 0.3%, leakage from the core material was observed due to cleavage on the coaxial interface. Therefore, coaxial-printed filaments could not be durably printed with 0.0% and 0.3% $CaCl_2$. In contrast, coaxial printability of shell material containing 0.2%

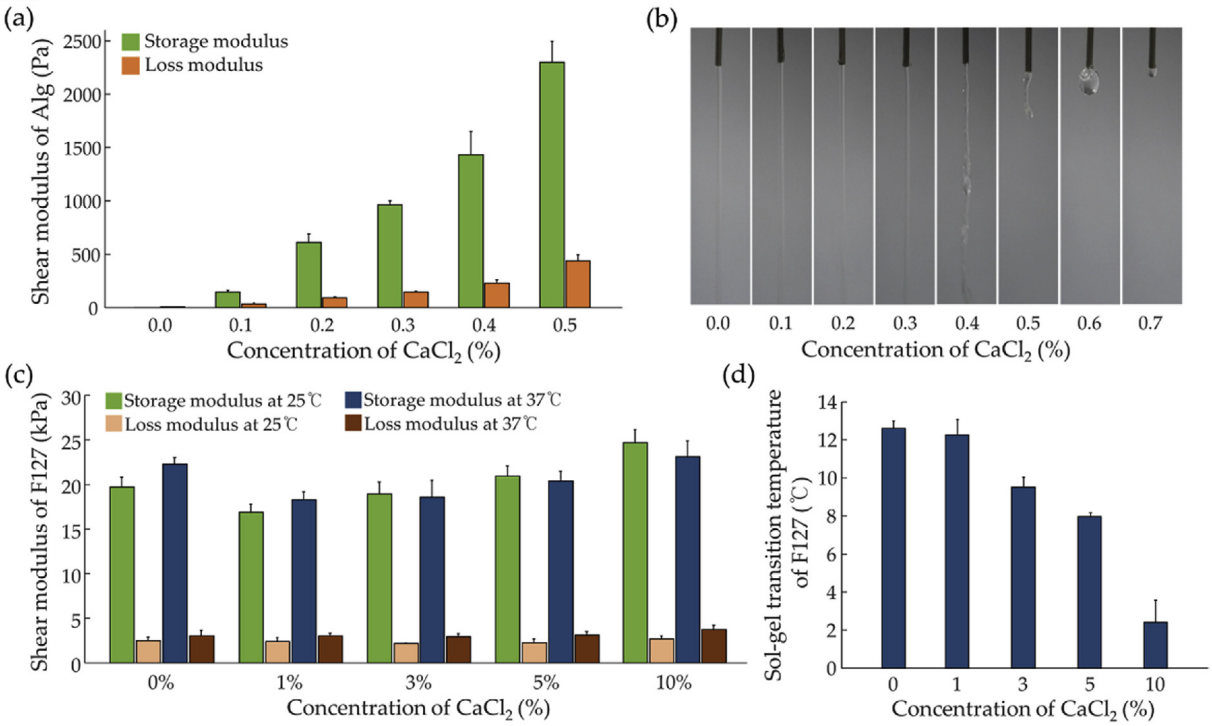

Fig. 2. Rheological properties of the biomaterials for bioprinting with various concentrations of $CaCl_2$: (a) Shear moduli of the crosslinked Alg solutions; (b) Extrudability of crosslinked Alg gels with $CaCl_2$ at 200 kPa using a single needle having a size of 340 μm (Detail with video in Video S1, Supplementary Materials); (c) Shear moduli of F127 with $CaCl_2$ at 25 °C and 37 °C; (d) Sol-gel transition temperature of F127 with various concentrations of $CaCl_2$.

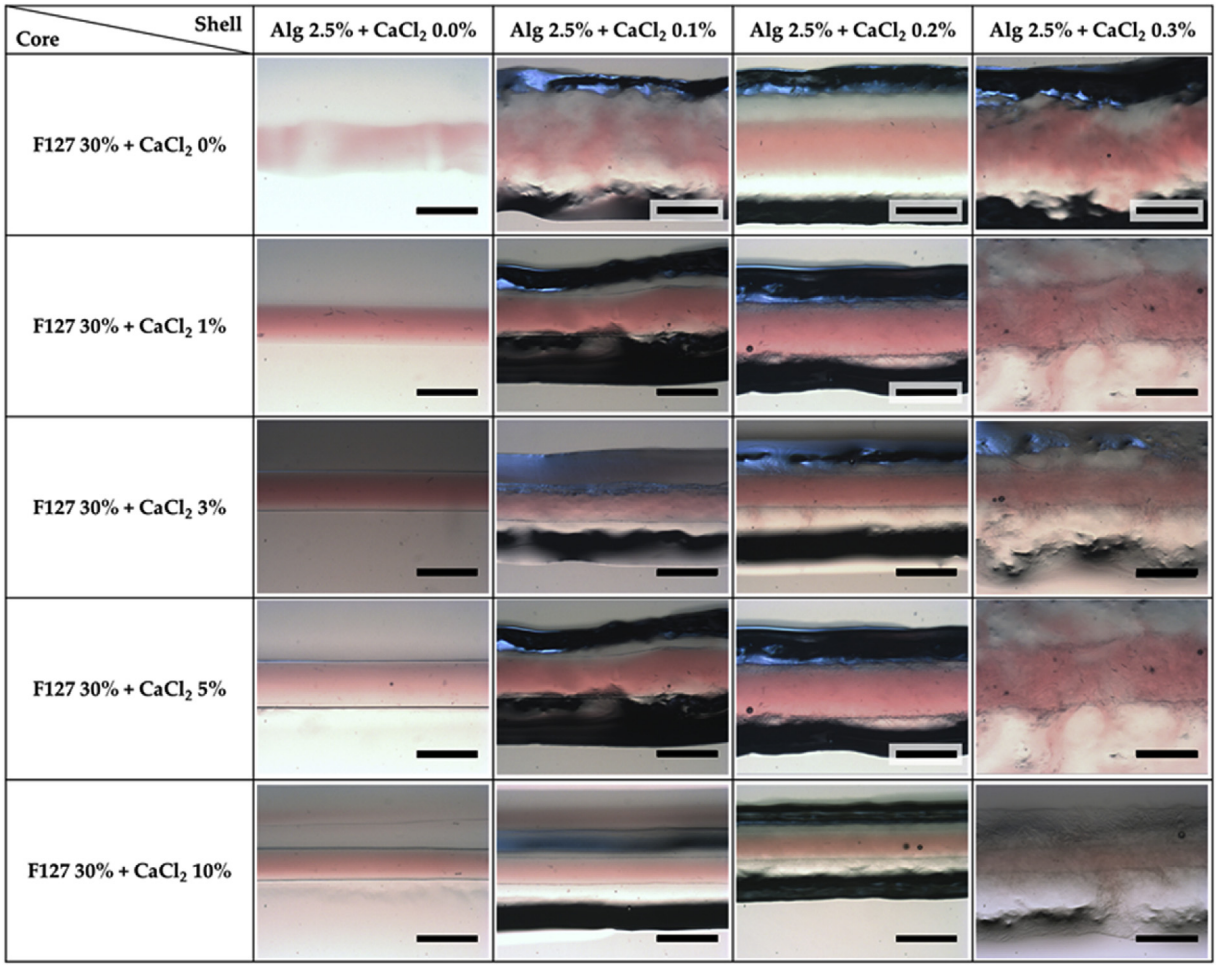

Fig. 3. Microscopic images of the coaxial-printed filaments with various combinations of $CaCl_2$ concentrations in shell and core materials (scale bar: 500 μm).

$CaCl_2$ was better than 0.1% $CaCl_2$. Also, it was confirmed that the extrusion uniformity and the morphological shape were firmed and closed to the straight line when the core material contained over 5% $CaCl_2$ and the shell material with 0.2% $CaCl_2$.

3.3. Structural integrity of the coaxial filament

The filament collapse test can assess structural integrity of the coaxial filaments fabricated with various combinations of $CaCl_2$ in shell and core materials as shown in Fig. 4. In the case of insufficient crosslinking of Alg by $CaCl_2$ resulting in the weakness of coaxial-printed filament, the degree of sagging is apparent as the distance of spacing increases for the filament collapse test. Likewise, in the shell material without $CaCl_2$, the pre-crosslinking was not conducted properly. Therefore, even if the concentration of $CaCl_2$ in the core material for the post-crosslinking is increased, the non-crosslinked Alg solution remained in droplets on the surface of the filament. However, the filament with 0.3% $CaCl_2$ in the shell material, there was a leakage in the filament due to excessive crosslinking occurring over-polymerization so that the red ink of the core material was released likewise in Fig. 3. Therefore, even though the printed filament with 3% $CaCl_2$ in the core part and 0.3% $CaCl_2$ in the shell part was likely to maintain well than the filament with 5% $CaCl_2$ in the core part, all the structures of the groups with 3% $CaCl_2$ in the core part had the cleavage between the coaxial interfaces. Also, the degree of sagging was increased in the group of 0% and 3% $CaCl_2$ in the shell material. In contrast, the shell materials with 0.1% and 0.2% $CaCl_2$ had relatively superb sagging strength of the coaxial-printed filaments. Furthermore, the post-crosslinking with 0.1% and 0.2% $CaCl_2$ was appropriately occurred at the core materials with 5% and 10% of $CaCl_2$ in both. In addition, no sagging, leakage, and no non-crosslinked Alg were observed from the coaxial-printed filament despite being tested on the widest spacing of the model. As a result, Alg 2.5% + $CaCl_2$ 0.2% was fixed as the shell material for the subsequent experiments.

3.4. Shape fidelity of coaxial-printed scaffolds

The shape fidelity of coaxial-printed scaffolds was compared with different concentrations of $CaCl_2$ in the core material with fixed shell material of Alg 2.5% + $CaCl_2$ 0.2%. The shape fidelity of the scaffold was monitored before (Fig. 5(a)) and after (Fig. 5(b)) removing the core material. In Fig. 5(a), the interface between the shell and core of the filament was indistinguishable when $CaCl_2$ was not contained in the core material. In the case of over 1% of $CaCl_2$ in the core material, the coaxial interface of the scaffold was distinct. However, in the macroscopic image, the red ink from the core material was leaked from the non-crosslinked part. The core material including 3% $CaCl_2$ achieved better coaxial encapsulation than 1% or less $CaCl_2$, but it was also difficult to fabricate a completely closed filament. Also, as shown in the microscopic image of the six-layered scaffold, pores of the scaffold were closed as a result of non-crosslinked Alg and leaked from the core material under 3% $CaCl_2$ in the core material. On the other hand, in 5% and 10% $CaCl_2$, coaxial-printed scaffolds could be successfully fabricated. However, 10% $CaCl_2$ in the core material results in the shrinkage of the printed scaffold due to excessive post-crosslinking. Thus, it was confirmed that the morphology of the pore was uncertain in the microscopic image of the six-layered scaffold with 10% $CaCl_2$.

(a)

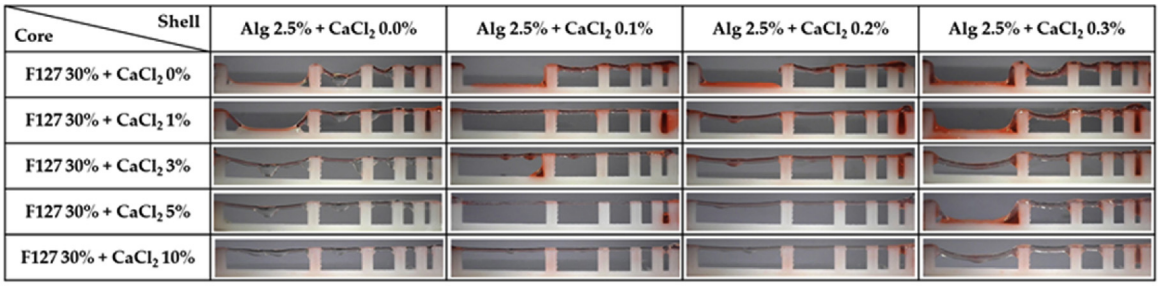

(b)

Core \ Shell	Alg 2.5% + $CaCl_2$ 0.0%			Alg 2.5% + $CaCl_2$ 0.1%			Alg 2.5% + $CaCl_2$ 0.2%			Alg 2.5% + $CaCl_2$ 0.3%		
	16 mm	8 mm	4 mm	16 mm	8 mm	4 mm	16 mm	8 mm	4 mm	16 mm	8 mm	4 mm
F127 30% + $CaCl_2$ 0%	77.77	58.13	37.35	N/A	15.9	9.81	N/A	20.44	5.1	57.62	45	22.83
F127 30% + $CaCl_2$ 1%	59.53	19.44	13.13	2.97	5.1	7.6	13.47	3.64	2.1	64.44	20.43	8.75
F127 30% + $CaCl_2$ 3%	24.54	15.15	10.3	2.66	2.16	1.43	6.8	2.58	2.54	37.12	16.59	4.64
F127 30% + $CaCl_2$ 5%	9.46	8.91	4.49	1.16	1.43	1.3	5.78	2.54	1.02	53.75	15.27	5.83
F127 30% + $CaCl_2$ 10%	4.5	3.22	3.58	1.94	0.4	1.41	4.03	1.05	0.77	30.26	9.82	3.3

Fig. 4. (a) Structural deformation of coaxial-printed filaments at 120 s after printing (Detail with various time points in Fig. S1, Supplementary Materials); (b) The degree of sagging of struts printed on the model for filament collapse test with 4 mm, 8 mm, and 16 mm spacing.

Fig. 5(b) presented the shape fidelity of the scaffold after removing the core material by cooling for an hour at 4 °C. F127 exists in the liquid state at low temperature, while it turns into gel at body temperature [35]. The thermal-reversibility of the F127 allows the core material to be removed easily at low temperature after printing. When the core material contains 0% and 1% $CaCl_2$, the printed structures were completely destructed due to improper gelation as shown in Fig. 5(b). The core material containing 3% $CaCl_2$ also showed a weak interface. In contrast, the coaxial-printed filament with 5% and 10% $CaCl_2$ in the core material could be clearly shown the coaxial interface as well as maintained the structures.

The inner and outer diameter of the coaxial-printed scaffolds were examined as shown in Fig. 5(c). It was determined that the inner diameters of the coaxial-printed scaffolds with 3%, 5%, and 10% $CaCl_2$ in the core part were 378 ± 18 μm, 462 ± 15 μm, and 333 ± 12 μm, respectively. Also, the outer diameters of each scaffold were 1019 ± 22 μm, 977 ± 34 μm, and 969 ± 20 μm, respectively. The coaxial-printed scaffold with 5% $CaCl_2$ had the smallest difference between the inner and the outer diameters, and it represents that the firm coaxial interface was obtained [37]. However, in general, it has been reported that excessive concentrations of $CaCl_2$ will affect biological problem such as cell viability [32]. Therefore, because coaxial printed scaffolds with 5% and 10% $CaCl_2$ in the core material were not significantly different, 5% $CaCl_2$ in the core material was selected for the coaxial printing in this experiment.

3.5. Comparison of the core-crosslinking method with the conventional method

The conventional crosslinking methods [32,33] for gelation of Alg were compared with the core-crosslinking method presented in this paper. In the conventional method, the Alg solution is mixed with $CaCl_2$ at a low concentration as a pre-crosslinking to increase the viscosity. Then, post-crosslinking with a high concentration of $CaCl_2$ is treated to maintain the 3D-printed Alg scaffold. Therefore, for the conventional method applied in this experiment, $CaCl_2$ was not contained to the core material, and the coaxial-printed scaffold was immersed in 5% $CaCl_2$ solution for a minute and washed three times using PBS. On the core-crosslinking method proposed in this paper was printed with the core material containing 5% $CaCl_2$. For both methods, the coaxial-printed scaffolds were immersed in PBS as in the same method of previous experiment to remove the core material and cured for an hour at 4 °C. In the photographic image as shown in Fig. 6A(a) and A(b), there was no significant difference. However, the microscopic image in Fig. 6A(c) showed that the crosslinked scaffold with the conventional method did not crosslink immediately and the boundaries of the coaxial-printed filament were not uniform. However, the other scaffold fabricated with the core-crosslinking method showed well-preserved shape fidelity of coaxial filament as shown in Fig. 6A(d). As shown in Fig. 6B, the scaffold fabricated by the conventional method had 641 ± 15 μm of inner diameter and 1036 ± 65 μm of outer diameter. Also, the scaffold produced with the core-crosslinking method had the inner and outer diameters of 462 ± 15 μm and 977 ± 33 μm, respectively. The result described that the core-crosslinking method allows the coaxial scaffold to have a well-organized structure than a conventionally fabricated scaffold. Due to $CaCl_2$ in the core material, Alg hydrogel was directly and uniformly crosslinked at each location and maintained its structure without additional crosslinking method.

4. Discussion

Recently, coaxial printing has investigated as a way to resolve the shortcomings of single nozzle printing [4,5,14]. The coaxial-printed structure allows the bioprinted-structure to have better cell attachment, proliferation, and differentiation than the normal bioprinted scaffold [5]. Also, by providing biochemical factors or oxygen into the hollow structure, the coaxial-printed structure enhances the tissue vascularization [6]. Despite the development of coaxial-printed structures for each application, developing a well-organized 3D coaxial structure is still challenging and has not been demonstrated, to the best of our knowledge. Therefore, methods that are capable of successful coaxial printing with a highly organized structure are strongly desired. In this regard, this study aims to improve the coaxial printability of biomaterials for coaxial printing and suggest the core-crosslinking method.

The coaxial-printed structure with improved structural integrity was fabricated using the core-crosslinking method with the optimal concentrations of $CaCl_2$ in alginate and Pluronic F-127 for shell and core parts, respectively. The well-constructed hollow structures developed by the core-crosslinking method would help to provide tubular histological structures with remarkable structural integrity. Also, by applying different diffusion rates for the core and shell parts, the inner and outer

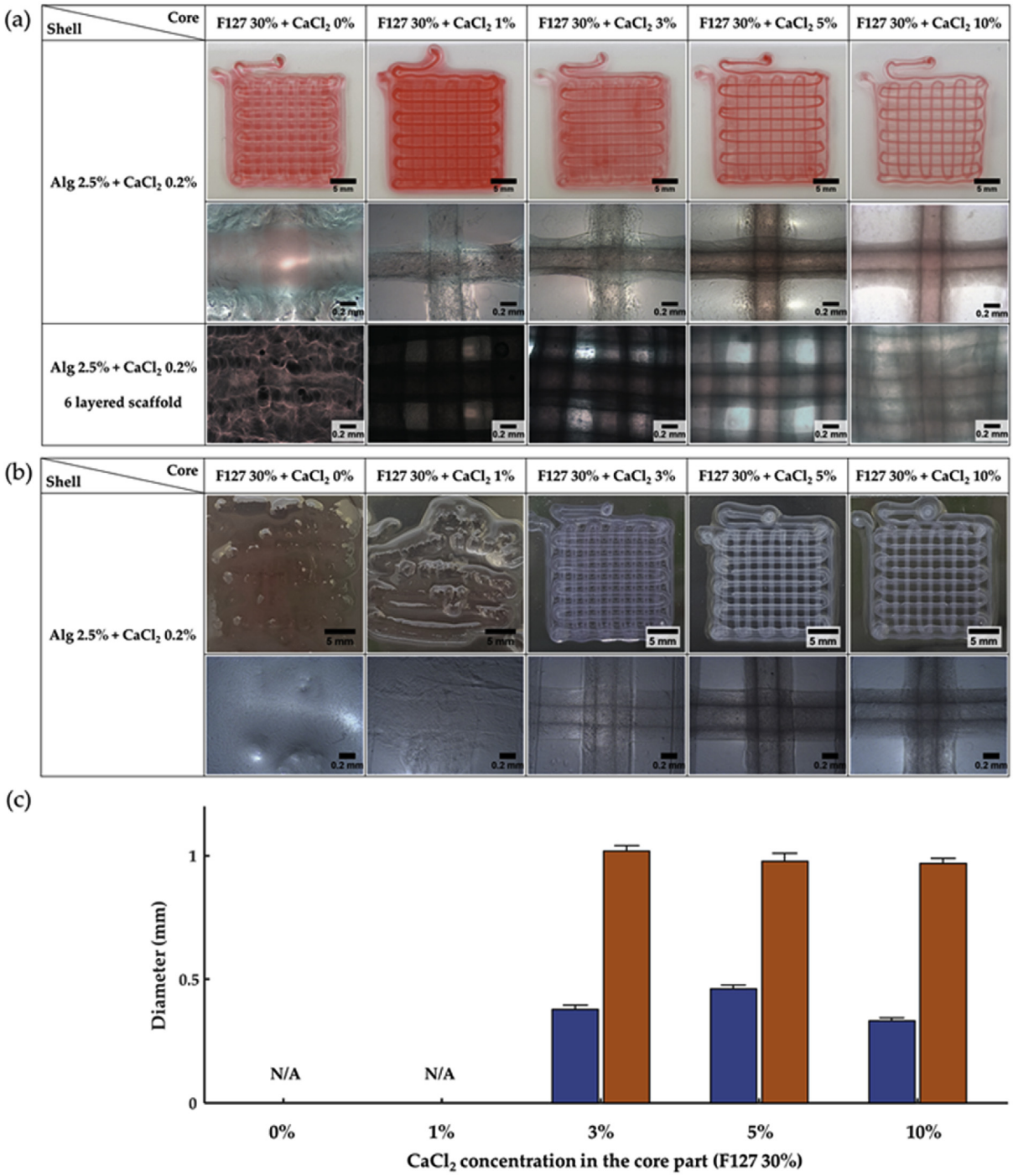

Fig. 5. Macroscopic and microscopic images of coaxial-printed scaffolds having two and six layers (a) before and (b) after the removal of the core material (F127); (c) Inner and outer diameters with different concentrations of $CaCl_2$ in the core part (n = 5).

diameters would be controlled suitable for various experiments.

The materials used in the study such as alginate, Pluronic F-127, and $CaCl_2$ have been proved that they are biocompatible and widely used in the field of biomedical applications [20,32,33,38]. However, to apply the core-crosslinking method to various tissue engineering applications for mimicking hollow tissue structures such as vasculature, trachea, or gastrointestinal tract, which are required a hollow structure for tissue regeneration, several biological experiments needs to be further evaluated. In our next step, we plan to study the biological interactions within the coaxial-printed structures fabricated by the core-crosslinking method through the in-depth in vitro study.

5. Conclusion

In this study, a coaxial-printed scaffold was successfully fabricated with high shape fidelity, by using alginate and Pluronic F-127 in the shell and core parts respectively. Also, the optimal concentrations of $CaCl_2$ for the pre-crosslinking and the post-crosslinking were quantitatively and

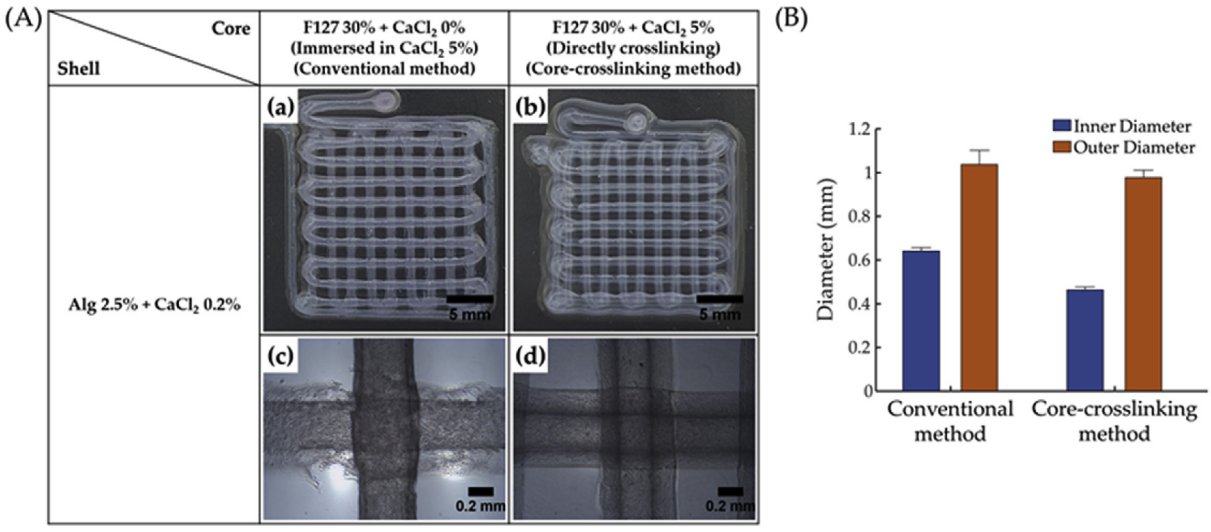

Fig. 6. Comparison of crosslinking methods between conventional and core-crosslinking after removal of the core material (F127) at 4 °C for an hour: (A) (a and c) Conventional crosslinking method using 5% $CaCl_2$ after coaxial printing; (b and d) Core-crosslinking method using 5% $CaCl_2$ included in the core; (B) Measurement of inner and outer diameter (n = 5).

comprehensively determined for fully-closed structure. Thus, the coaxial printability and shape fidelity were assessed and was best at Alg 2.5% + $CaCl_2$ 0.2% for the shell material and F127 30% + $CaCl_2$ 5% for the core material. With the optimal concentration of $CaCl_2$ for Alg, the shell and core materials for coaxial printing could be used to directly fabricate a 3D tubular structure with high resolution for various applications in tissue engineering and regenerative medicine. Further, this investigation could serve a methodological solution for improving the coaxial printability and enhance the shape fidelity of the coaxial-printed structure with optimal concentrations of the biomaterials.

CRediT authorship contribution statement

Myoung Hwan Kim: Conceptualization, Methodology, Visualization, Investigation, Validation, Writing - original draft. **Seung Yun Nam:** Supervision, Conceptualization, Validation, Funding acquisition, Writing - review & editing.

Declaration of competing interest

The authors declare that they have no known competing financial interests or personal relationships that could have appeared to influence the work reported in this paper.

Acknowledgement

This work was supported by a Research Grant of Pukyong National University (2019).

Appendix A. Supplementary data

Supplementary data to this article can be found online at https://doi.org/10.1016/j.bprint.2020.e00092.

References

[1] I.T. Ozbolat, K.K. Moncal, H. Gudapati, Evaluation of bioprinter technologies, Addit. Manuf. 13 (2017) 179–200.
[2] M.H. Kim, C. Yun, E.P. Chalisserry, Y.W. Lee, H.W. Kang, S.-H. Park, W.-K. Jung, J. Oh, S.Y. Nam, Quantitative analysis of the role of nanohydroxyapatite (nHA) on 3D-printed PCL/nHA composite scaffolds, Mater. Lett. 220 (2018) 112–115.
[3] W. Liu, M.A. Heinrich, Y. Zhou, A. Akpek, N. Hu, X. Liu, X. Guan, Z. Zhong, X. Jin, A. Khademhosseini, Extrusion bioprinting of shear-thinning gelatin methacryloyl bioinks, Adv. Healthc. Mater. 6 (2017) 1601451.
[4] W. Liu, Z. Zhong, N. Hu, Y. Zhou, L. Maggio, A.K. Miri, A. Fragasso, X. Jin, A. Khademhosseini, Y.S. Zhang, Coaxial extrusion bioprinting of 3D microfibrous constructs with cell-favorable gelatin methacryloyl microenvironments, Biofabrication 10 (2018), 024102.
[5] M. Yeo, J.-S. Lee, W. Chun, G.H. Kim, An innovative collagen-based cell-printing method for obtaining human adipose stem cell-laden structures consisting of core–sheath structures for tissue engineering, Biomacromolecules 17 (2016) 1365–1375.
[6] W. Zhang, C. Feng, G. Yang, G. Li, X. Ding, S. Wang, Y. Dou, Z. Zhang, J. Chang, C. Wu, 3D-printed scaffolds with synergistic effect of hollow-pipe structure and bioactive ions for vascularized bone regeneration, Biomaterials 135 (2017) 85–95.
[7] J. Malda, J. Visser, F.P. Melchels, T. Jüngst, W.E. Hennink, W.J. Dhert, J. Groll, D.W. Hutmacher, 25th anniversary article: engineering hydrogels for biofabrication, Adv. Mater. 25 (2013) 5011–5028.
[8] B.A. Aguado, W. Mulyasasmita, J. Su, K.J. Lampe, S.C. Heilshorn, Improving viability of stem cells during syringe needle flow through the design of hydrogel cell carriers, Tissue Eng. A 18 (2011) 806–815.
[9] D. Chimene, K.K. Lennox, R.R. Kaunas, A.K. Gaharwar, Advanced bioinks for 3D printing: a materials science perspective, Ann. Biomed. Eng. 44 (2016) 2090–2102.
[10] Y. Kim, G. Kim, Collagen/alginate scaffolds comprising core (PCL)–shell (collagen/alginate) struts for hard tissue regeneration: fabrication, characterisation, and cellular activities, J. Mater. Chem. B 1 (2013) 3185–3194.
[11] L. Moroni, J. Hendriks, R. Schotel, J. De Wijn, C. Van Blitterswijk, Design of biphasic polymeric 3-dimensional fiber deposited scaffolds for cartilage tissue engineering applications, Tissue Eng. 13 (2007) 361–371.
[12] F. Dolati, Y. Yu, Y. Zhang, A.M. De Jesus, E.A. Sander, I.T. Ozbolat, In vitro evaluation of carbon-nanotube-reinforced bioprintable vascular conduits, Nanotechnology 25 (2014) 145101.
[13] A.-V. Do, A. Akkouch, B. Green, I. Ozbolat, A. Debabneh, S. Geary, A.K. Salem, Controlled and sequential delivery of fluorophores from 3D printed alginate-PLGA tubes, Ann. Biomed. Eng. 45 (2017) 297–305.
[14] W. Jia, P.S. Gungor-Ozkerim, Y.S. Zhang, K. Yue, K. Zhu, W. Liu, Q. Pi, B. Byambaa, M.R. Dokmeci, S.R. Shin, Direct 3D bioprinting of perfusable vascular constructs using a blend bioink, Biomaterials 106 (2016) 58–68.
[15] X. Liu, S.S.D. Carter, M.J. Renes, J. Kim, D.M. Rojas-Canales, D. Penko, C. Angus, S. Beirne, C.J. Drogemuller, Z. Yue, Development of a Coaxial 3D Printing Platform for Biofabrication of Implantable Islet-Containing Constructs, Advanced Healthcare Materials, 2019, p. 1801181.
[16] X. Dai, L. Liu, J. Ouyang, X. Li, X. Zhang, Q. Lan, T. Xu, Coaxial 3D bioprinting of self-assembled multicellular heterogeneous tumor fibers, Sci. Rep. 7 (2017) 1457.
[17] L. Ouyang, R. Yao, Y. Zhao, W. Sun, Effect of bioink properties on printability and cell viability for 3D bioplotting of embryonic stem cells, Biofabrication 8 (2016), 035020.
[18] J.H. Chung, S. Naficy, Z. Yue, R. Kapsa, A. Quigley, S.E. Moulton, G.G. Wallace, Bio-ink properties and printability for extrusion printing living cells, Biomater. Sci. 1 (2013) 763–773.
[19] A.C. Taylor, S. Beirne, G. Alici, G.G. Wallace, System and process development for coaxial extrusion in fused deposition modelling, Rapid Prototyp. J. 23 (2017) 543–550.

[20] D.B. Kolesky, R.L. Truby, A.S. Gladman, T.A. Busbee, K.A. Homan, J.A. Lewis, 3D bioprinting of vascularized, heterogeneous cell-laden tissue constructs, Adv. Mater. 26 (2014) 3124–3130.
[21] D.G. Karis, R.J. Ono, M. Zhang, A. Vora, D. Storti, M.A. Ganter, A. Nelson, Cross-linkable multi-stimuli responsive hydrogel inks for direct-write 3D printing, Polym. Chem. 8 (2017) 4199–4206.
[22] Y. Jun, E. Kang, S. Chae, S.-H. Lee, Microfluidic spinning of micro-and nano-scale fibers for tissue engineering, Lab Chip 14 (2014) 2145–2160.
[23] A. Panwar, L.P. Tan, Current status of bioinks for micro-extrusion-based 3D bioprinting, Molecules 21 (2016) 685.
[24] M.H. Kim, Y.W. Lee, W.-K. Jung, J. Oh, S.Y. Nam, Enhanced rheological behaviors of alginate hydrogels with carrageenan for extrusion-based bioprinting, J. Mech. Behav. Biomed. Mater. 98 (2019) 187–194.
[25] S.E. Bakarich, R. Gorkin III, R. Gately, S. Naficy, M. in het Panhuis, G.M. Spinks, 3D printing of tough hydrogel composites with spatially varying materials properties, Addit. Manuf. 14 (2017) 24–30.
[26] D. Therriault, S.R. White, J.A. Lewis, Rheological behavior of fugitive organic inks for direct-write assembly, Appl. Rheol. 17 (2007) 10112–11411.
[27] A. Habib, V. Sathish, S. Mallik, B. Khoda, 3D printability of alginate-carboxymethyl cellulose hydrogel, Materials 11 (2018) 454.
[28] A. Ribeiro, M.M. Blokzijl, R. Levato, C.W. Visser, M. Castilho, W.E. Hennink, T. Vermonden, J. Malda, Assessing bioink shape fidelity to aid material development in 3D bioprinting, Biofabrication 10 (2017), 014102.
[29] S. Ahn, H. Lee, E.J. Lee, G. Kim, A direct cell printing supplemented with low-temperature processing method for obtaining highly porous three-dimensional cell-laden scaffolds, J. Mater. Chem. B 2 (2014) 2773–2782.
[30] B. Duan, L.A. Hockaday, K.H. Kang, J.T. Butcher, 3D bioprinting of heterogeneous aortic valve conduits with alginate/gelatin hydrogels, J. Biomed. Mater. Res. 101 (2013) 1255–1264.
[31] I.T. Ozbolat, H. Chen, Y. Yu, Development of 'Multi-arm Bioprinter'for hybrid biofabrication of tissue engineering constructs, Robot. Comput. Integrated Manuf. 30 (2014) 295–304.
[32] S. Ahn, H. Lee, L.J. Bonassar, G. Kim, Cells (MC3T3-E1)-laden alginate scaffolds fabricated by a modified solid-freeform fabrication process supplemented with an aerosol spraying, Biomacromolecules 13 (2012) 2997–3003.
[33] S. Ahn, H. Lee, J. Puetzer, L.J. Bonassar, G. Kim, Fabrication of cell-laden three-dimensional alginate-scaffolds with an aerosol cross-linking process, J. Mater. Chem. 22 (2012) 18735–18740.
[34] A.C. Bierhalz, M.A. da Silva, M.E. Braga, H.J. Sousa, T.G. Kieckbusch, Effect of calcium and/or barium crosslinking on the physical and antimicrobial properties of natamycin-loaded alginate films, LWT-Food Sci. Technol. 57 (2014) 494–501.
[35] P.T. Smith, A. Basu, A. Saha, A. Nelson, Chemical modification and printability of shear-thinning hydrogel inks for direct-write 3D printing, Polymer 152 (2018) 42–50.
[36] J. Jiang, C. Li, J. Lombardi, R.H. Colby, B. Rigas, M.H. Rafailovich, J.C. Sokolov, The effect of physiologically relevant additives on the rheological properties of concentrated Pluronic copolymer gels, Polymer 49 (2008) 3561–3567.
[37] Y. Zhang, Y. Yu, H. Chen, I.T. Ozbolat, Characterization of printable cellular micro-fluidic channels for tissue engineering, Biofabrication 5 (2013), 025004.
[38] M. Hospodiuk, M. Dey, D. Sosnoski, I.T. Ozbolat, The bioink: a comprehensive review on bioprintable materials, Biotechnol. Adv. 35 (2017) 217–239.